Materials Sciences and Applications, 2022, 13, 532-557
https://www.scirp.org/journal/msa
ISSN Online: 2153-1188
ISSN Print: 2153-117X

Synthesis and Physicochemical Studies for Novel Bioactive Metal Complexes of Macrolide Antibiotic Tylosin

Alaa E. Ali[1], Gehan S. Elasala[1], Yasser S. Mahrous[1], Mohamed H. Sharaf[2], Ismael M. Elkamhawy[1*]

[1]Chemistry Department, Faculty of Science, Damanhour University, Damanhour, Egypt
[2]Botany and Microbiology Department, Faculty of Science, Al-Azhar University, Cairo, Egypt
Email: *Ismael.elkamhawy@sci.dmu.edu.eg, *Ismaelelkamhawy@gmail.com

How to cite this paper: Ali, A.E., Elasala, G.S., Mahrous, Y.S., Sharaf, M.H. and Elkamhawy, I.M. (2022) Synthesis and Physicochemical Studies for Novel Bioactive Metal Complexes of Macrolide Antibiotic Tylosin. *Materials Sciences and Applications*, **13**, 532-557.
https://doi.org/10.4236/msa.2022.1310033

Received: August 3, 2022
Accepted: October 28, 2022
Published: October 31, 2022

Abstract

Tylosin is a well-established antibiotic that has been widely employed in human and veterinary medicines. It can act as a potential ligand binding metal ions due to various donor atoms in the structure. Our study on the complexation of various metal ions with tylosin ligand revealed that they preferably coordinate with mycaminose fragment to establish Novel trends complexes. Tylosin ligand (TYS) behaves as bidentate for complexation with different metal ions such as Cr(III), Mn(II), Fe(III), Co(II), Ni(II), Cu(II) and Zn(II). Various essential metal complexes of tylosin were synthesized and characterized by techniques such as UV, IR, Elemental analysis, magnetic susceptibility and ESR spectra of Cu(II) complex. These techniques are used to know their geometries and mode of bonding, with stoichiometry, 2:2 (M:L). Thermal analysis (TGA and DTA) of ligands and their metal complexes were carried out to distinguish between the coordinate and hydrate solvents and to estimate the stability ranges, peak temperatures. The thermodynamic parameters, such as activation energy (ΔE^*), the enthalpy of activation (ΔH^*), entropy of activation (ΔS^*) and Gibbs free energy (ΔG^*) are calculated and discussed. Some tylosin complexes show higher activity than tylosin for some bacterial and fungal strains. Low concentration value of minimum inhibitory concentration (MIC) results is 15.625 μg/ml for both complexes $[Zn_2(TYS)_2Cl_2(H_2O)_4]\cdot 25H_2O$ and $[Cu_2(TYS)_2Cl_2(H_2O)_4]\cdot 25H_2O$ with *B. cereus* genus maybe a valuable data used to produce novel therapeutic agent. This study constitutes several essential aspects for future research on tylosin metal complexes as antibacterial assessment and as potential medicinal agents.

Keywords

Tylosin Complexes, Synthesis, Spectral, Tetragonal Distortion,

Biological Activity

1. Introduction

Tylosin (TYS), a macrolide antibiotic, is produced naturally by the Actinomycetota species *Streptomyces fradiae*, which was firstly identified by McGuire in 1961 [1]. Tylosin (**Figure 1**) is a 16-membered branched lactone, tylonolide, with disaccharide (*α*-L-mycarosyl*β*-D-mycaminosyl) and monosaccharide (*α*-D-mycinose) substituents. Tylosin (TYS) mostly consists of tylosin (factor A), but it may also contain small amounts of desmycosin (factor B), macrocin (factor C), and relomycin (factor D) and tylosin (A) being at least 80% of the composition [2] [3]. Tylosin (TYS) has significant commercial importance which is used effectively as a veterinary medication and feed additive to stimulate young animals' growth. It is highly effective against both Gram-positive and Gram-negative bacteria as well as Gram-positive mycoplasmas. Tylosin is typically reported to be less active against most bacteria, with the exception of Mycoplasma species, as compared to erythromycin (a prototypical macrolide molecule). In ruminants, pigs, and poultry, antibiotic is used to treat a variety of illnesses brought on by sensitive organisms [4] [5]. The wide use of tylosin antibiotic from the macrolide series makes it crucial to regulate their concentration in both dosage forms and biological liquids [6]. Currently, techniques like liquid chromatography [7], high performance liquid chromatography (HLPC) [8] [9] [10] and spectrophotometric methods [11] are employed to identify macrolide antibiotics. Tylosin (TYS) is White to buff-colored powder with a mild musty odor; its melting point is "128˚C - 132˚C" and its solubility in water 5 mg/mL at 25˚C and Freely soluble in methanol. Soluble in lower alcohols, esters and ketones, chloroform, dilute mineral acids, amyl acetate, chlorinated hydrocarbons, benzene, and ether. Tylosin is unstable in acidic and alkaline medium and relatively stable under neutral pH conditions (pH = 7). It is chemically stable under standard ambient conditions (room temperature) [12]. Antibiotic resistance is growing at an alarming

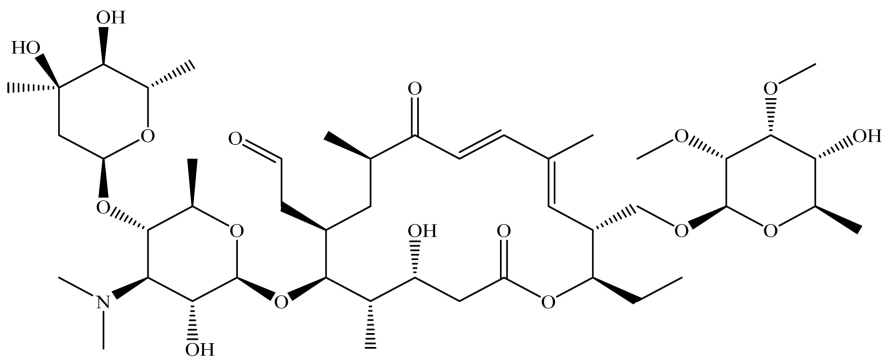

Chemical Formula: $C_{46}H_{77}NO_{17}$
Molecular Weight: 916.11

Figure 1. The chemical structure of tylosin A (TYS).

rate and consequently the activity of antibiotics against Gram-positive and Gram-negative bacteria is becoming less effective gradually day by day. In a concrete sense, there is a considerable need for the design of novel antibiotics therapeutic with a good spectrum of activity, so the current study framework is to establish a foundation for antimicrobials.

2. Experimental

Tylosin was dissolved in distilled water, while metal chlorides of Cr(III), Mn(II), Fe(III), Co(II), Ni(II), Cu(II), and Zn(II) were dissolved in ethanol 70%, then several molar ratios were tested until reach to the stoichiometry of (M:L). 40 ml of dissolved heated ethanol solution of chlorides inorganic salts of transition metal ions mixed with water soluble tylosin ligand. The reaction mixture was refluxed for approximately 60 minutes and then allowed to sit overnight. The high yield precipitated complexes were determined to identify the molar ratio of the predicted amount of ligand and the molar amount of the metal chloride salt interacted. The synthesized complexes were then filtered, washed several times with a 70% ethanol solution, and dried in a vacuum desiccator over anhydrous $CaCl_2$.

3. Measurements

3.1. Elemental Analysis and Physical Measurements

The metal contents were determined by atomic absorption spectrophotometer. Carbon, hydrogen and nitrogen analysis of tylosin and all complexes measured at central lab, Cairo University contents of all the synthesized complexes were analyzed by the usual method. The well-known Volhard method [13] was used in an acidic medium to analyze the complexes' chloride contents. Melting points were measured by using the FALC melting point device.

3.2. Spectral Studies

The infrared spectra of tylosin and its metal complexes were obtained in a KBr disc using The Bruker Tensor 37 FT-IR instrument which is located in the central lab, Alexandria university, covering frequency range of 400 - 4000 cm^{-1} and the data recorded and refined by OPUS Data Collection Program.

Electronic spectra of the colored complexes were detected in nujol mull spectra following the method described by Lee, Griswold and Kleinberg [14] using Perkin Elmer lambda 25 uv/vis spectrophotometer, made in England that can Detect the wavelengths between 190 - 1100 nm.

ESR spectra of Cu(II) tylosin complex was measured on an ERS-220 X-band spectrometer (9.45 GHz) using 100-kHz field modulation at room temperature and at 77˚K; g factors were determined in relation to the reference marker DPPH ($g = 2.0036$).

Magnetic susceptibility measurements were measured at room temperature on a Johnson Matthey magnetic susceptibility balance using Gouy method. Diamagnetic corrections were calculated using Pascal's constants [15]; the calibrant

used was $Hg[Co(SCN)_4]$. The values of effective magnetic moments were calculated from the following equation $\mu_{\text{eff}} = 2.84\left(X_M^{corrt}T\right)^{1/2}$, where, X_M^{corrt} is the molar magnetic susceptibility corrected for diamagnetism of all atoms in the compounds.

3.3. Thermo Gravimetric Analysis (TG) and Differential Thermal Analysis (DTA)

Differential thermal analysis (DTA) and thermo gravimetric analysis (TG) of tylosin and its metal complexes were carried out using the instrument LINSEIS PT1600. The rate of heating was 10˚ K/min. The cell used was platinum and the atmospheric nitrogen rate flow was 15 ml/min.

3.4. Biological Studies

The antimicrobial activity of the tested compounds were determined by means of paper disk diffusion method (7 mm) on Muller Hinton agar for bacteria and potato dextrose agar for Candida [16]. The bacterial indicators were *S. aureus* (ATCC6538), *B. cereus* (ATCC10987), for Gram-positive bacteria, *E. coli* (ATCC 8739), *S. Typhi* (ATCC14028) as Gram-negative bacteria and one fungal strain *C. albicans* (ATCC10231).

The minimum inhibitory concentration (MIC) carried out by preparing Different concentrations of compounds. Test sample (100 µl) of various concentrations was added into sterile microtiter plate wells filled with 100 µl of double strength Mueller Hinton (MH) broth to make final concentrations at 1000, 500, 250, 125, 62.5, 31.25. and 15.75 µg/ml. Bacterial cell suspension (50 µl) corresponding to (OD equivalent to 0.5 McFarland standard) was added in all wells except those in the negative control well. Positive Control wells were filled with MH broth and bacterial suspension to check for adequacy of the broth to support bacteria growth [17]. The negative control wells consisted of sterile distilled water and Mueller Hinton broth to check sterility. The plates were incubated at 37˚C for 24 hrs. To indicate bacterial growth, 30 µl of resazurin solution (0.02% w/v) (HiMedia) was added to each well, and the plate was re-incubated overnight. A change in color from blue to purple, red or pink, indicated the growth of bacteria. A change in the color of growth control wells to pink, red or purple indicated the proper growth of the isolate and no change in the color of the sterile control well indicated the absence of contaminants. The experiment was performed in duplicates and mean values were calculated [18].

4. Results and Discussion

4.1. Elemental Analysis and Stoichiometry of Novel Tylosin Metal Complexes

The proportion of elements in the innovative metal complexes was determined and quantified by elemental analysis, **Table 1**; also certain characteristics such as color, Yield and chemical formula of tylosin macrolide ligand and its metal

Table 1. Indicated elemental analysis, molecular formula, stoichiometry's, yield and color of tylosin ligand and its metal complexes.

Compound	Empirical Formula Formula Weight (gm/mol)	Color	Yield (%)	Elemental Analysis, Calculated (Found) %				
				C	H	N	M	Cl
Tylosin (TYS·6.7H_2O) Ligand	$C_{46}H_{90.4}NO_{23.7}$ 1036.71	Buff	-	53.29 (53.74)	8.72 (8.62)	1.35 (1.24)	-	-
$[Fe_2(TYS)_2Cl_4(H_2O)_2]\cdot 26H_2O$ 2:2	$C_{92}H_{210}Cl_4Fe_2N_2O_{62}$ 2588.44	pale brown	89 %	42.69 (42.52)	8.11 (8.44)	1.08 (1.20)	4.31 (4.42)	5.48 (5.65)
$[Zn_2(TYS)_2Cl_2(H_2O)_4]\cdot 25H_2O$ 2:2	$C_{92}H_{212}Cl_2Zn_2N_2O_{63}$ 2554.60	Yellowish white	94 %	43.25 (43.01)	8.30 (8.45)	1.10 (1.22)	5.12 (4.92)	2.78 (2.72)
$[Mn_2(TYS)_2Cl_2(H_2O)_4]\cdot 22.4H_2O$ 2:2	$C_{92}H_{206.8}Cl_2N_2Mn_2O_{60.4}$ 2486.92	Wine-red	88 %	44.43 (44.18)	8.32 (8.40)	1.13 (1.22)	4.41 (4.28)	2.85 (2.75)
$[Cr_2(TYS)_2Cl_4(H_2O)_2]\cdot 27H_2O$ 2:2	$C_{92}H_{210}Cl_4Cr_2N_2O_{63}$ 2596.74	Dark green	83 %	42.55 (42.12)	8.09 (8.25)	1.08 (1.15)	4.00 (4.12)	5.46 (5.60)
$[Ni_2(TYS)_2(Cl)_2(H2O)_4]\cdot 28.8H_2O$ 2:2	$C_{92}H_{216.6}Cl_2N_2Ni_2O_{66.8}$ 2609.38	Pale green	92 %	42.39 (42.30)	8.31 (8.32)	1.07 (1.24)	4.50 (4.37)	2.72 (2.84)
$[Co_2(TYS)_2Cl_2(H_2O)_4]\cdot 18H_2O$ 2:2	$C_{92}H_{198}Cl_2Co_2N_2O_{56}$ 2415.71	Dark green	94 %	45.74 (45.62)	8.20 (8.26)	1.16 (1.23)	4.88 (5.00)	2.94 (2.75)
$[Cu_2(TYS)_2Cl_2(H_2O)_4]\cdot 25H_2O$ 2:2	$C_{92}H_{212}Cl_2Cu_2N_2O_{63}$ 2550.93	pale green	94 %	43.32 (43.10)	8.31 (8.36)	1.10 (1.12)	4.98 (5.00)	2.78 (2.65)

complexes are included. The analytical findings proved that the tylosin ligand reacts in 2:2 (M:L) molar ratio with Mn(II), Co(II), Ni(II), Cu(II), Zn(II), Fe(III) and Cr(III). The complexes are highly hydroscopic. All the complexes are slightly soluble in N,N-dimethylformamide (DMF) and highly soluble in dimethyl sulfoxide (DMSO-d6). While, in ethanol, methanol and water, all complexes are insoluble. All of the complexes had a melting point values greater than 325˚C.

4.2. Infrared (IR) Spectra of Tylosin and Its Metal Complexes

The infrared spectrum of tylosin was interpreted by correlating the functional groups it contains in the structure of molecule to the spectrum it produces [19] [20] [21]. Spectroscopic characteristics of tylosin (**Figure 2**) revealed an absorption band which is observed at 1720 cm^{-1} assigned to the lactone carbonyl group. The absorption bands at 1460, 1510 and 1560 cm^{-1} are associated with stretches vibrations of C=O and C=C. There are several absorption bands in the range of 1050 to 1300 cm^{-1} that are associated with the C-O group of the alcohol, ether, and ester functionalities. The C-N group promotes an absorption band in the 1180 - 1280 cm^{-1} range. The C=O group is connected to the bands of absorption that are related to the functions of ester, aldehyde and ketone at 1380 cm^{-1}, 1560 cm^{-1}, and between 1650 and 1750 cm^{-1}. The band around 1420 cm^{-1} is attributed

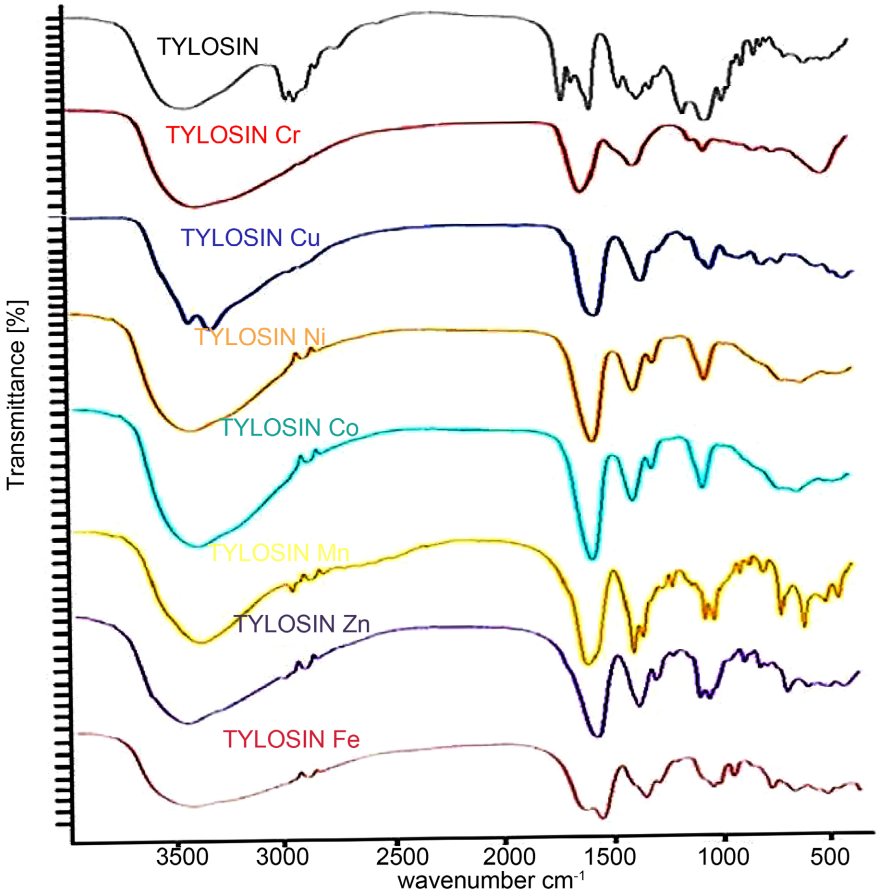

Figure 2. Infrared spectra of tylosin (TYS) ligand and its metal complexes.

to the angular deformation of CH_2 beside carbonyl. In the 1620 - 1680 cm^{-1} range, there are absorption bands related to C=C deformation. The absorption bands in the range of 2700 - 2960 cm^{-1} are related to the C-H group. Absorption bands in the region of 670 to 970 cm^{-1} are related to the CH=CH group. The OH group is responsible for the absorption band that spans the wavelengths of 3200 to 3600 cm^{-1}.

The infrared spectrum of tylosin metal complexes for Zn^{2+}, Cu^{2+}, Mn^{2+}, Co^{2+}, Ni^{2+}, Cr^{3+} and Fe^{3+} were recorded and then Compared to the IR spectrum of TYS ligand. The bands in the range (1720 - 1735) cm^{-1} were also noticed in the tylosin metal complexes spectral sheet, which was assigned to the lactone carbonyl group which is strong evidence that there is no coordination between the lactone carbonyl group and the metal ions. The main differences are changes in the relative intensity for OH group (3200 to 3600) cm^{-1}, which can conclude that metal ions coordinated with poly hydroxyl mycaminose fragment. The band at 1250 cm^{-1}, which assigned to C-N group in ligand spectral sheet, has been red shifted to the range 1125 - 1163 cm^{-1} which indicates that the metal ions may be bind with 3˚ amine donor group to form a stable metal complexes structure.

In the far IR spectra, the presence of M-N stretching vibration in the (510 - 585) cm^{-1} range which is absent in the free ligand provides evidence that moiety

is bonded to the metal ion through nitrogen. Also the new bands were detected in the range (440 - 485) cm^{-1} detected in the complexes assigned to M-O which confirmed the bonding of nitrogen and oxygen to metal ions.

4.3. Electronic Absorption Spectra and Magnetic Susceptibility Studies

Generally, the magnetic moment readings for metal ions at room temperature as well as the Nujol mull electronic spectral data of synthesized metal complexes have been applied to determine the possible geometry of these synthetic complexes. These measurements have been clarified in Table 2. However; each metal ion complex will be described and discussed independently as follows.

4.3.1. Nickel Complex

The values of μ_{eff} of Ni(II) complex $[Ni_2(TYS)_2(Cl)_2(H_2O)_4]$, at room temperature were found to be 3.20 BM which is higher than of $\mu_{s.o}$ value that is characterized for two unpaired electrons of Ni(II) octahedral complexes. The ensuing high value of magnetic moment may be a sign of Strong spin orbit coupling under which $\mu_{eff} = \mu_{S.O}.(1 - 4\lambda/10Dq)$. As the spin orbit coupling constant λ for d^8 system is ($\lambda = -315$), μ_{eff} becomes greater than $\mu_{S.O}$. Ni(II)-TYS complex shows four bands in their electronic spectra, suggesting distorted tetragonal geometry (D_{4h}). These bands can be assigned to the following transitions [22].

$$\nu_1 = {}^3B_{1g} \rightarrow {}^3E_g \qquad 10Dq - 35/4Dt$$

$$\nu_2 = {}^3B_{1g} \rightarrow {}^3B_{2g} \qquad 10Dq$$

$$\nu_3 = {}^3B_{1g} \rightarrow {}^3A_{2g} \qquad 18Dq - 4Ds - 5Dt$$

$$\nu_4 = {}^3B_{1g} \rightarrow {}^4E_g \qquad 18Dq - 2Ds - 25/4Dt$$

The tetragonal character is measured by the transition ${}^3B_{1g} \rightarrow {}^3E_g{}^{(a)}$. The transition ${}^3B_{1g} \rightarrow {}^3B_{2g}{}^{(b)}$, on the other hand, is unaffected by Ds and Dt while is effectively the measure of the infield splitting parameter Dq^{xy}. The axial distortion Dt is computed by using the Wentworth and Piper formula [23], which is $Dt = 4/7(Dq^{xy} - Dq^{Z})$ or by another derived formula $35/4Dt = \nu_2 - \nu_1$. The equation $2\nu_1 - \nu_2/10$ was used to compute Dq^{Z}. The zero field splitting parameter (D) has also been calculated using the expression $D = 9k_1/\alpha^2[(\mu_{eff}/\mu_{s.o})^2 - (\mu_{eff}/\mu_{s.o}) + 1S]$ while k_1, is the splitting of the initial excited state, and it is given as $k_1 = 35/4Dt$. The values for the various parameters are listed in Table 2. The presence of four bands indicates a significant tetragonal deviation from octahedral symmetry. The positive value of Dt, Ds and smaller value of Dq^z than Dq^{xy} are assigned to tetragonal elongated octahedral geometry of Ni(II) complex. The features of all produced bands that represent these complex transitions as shown in Figure 3 were in strong feature and well analyzed; the complex Ni(II)-TYS shows four bands at 1041.7, 941.6, 541.1 and 416.7 nm, which correspond to the transitions ${}^3B_{1g} \rightarrow {}^3E_g$ (υ_1), ${}^3B_{1g} \rightarrow {}^3B_{2g}$ (υ_2), ${}^3B_{1g} \rightarrow {}^3A_{2g}$ (υ_3) and ${}^3B_{1g} \rightarrow {}^4E_g$ (υ_4) respectively, that is a great elucidation of tetragonal elongated octahedral structure.

Table 2. Indicates Nujol mull electronic absorption spectra (nm·cm^{-1}), room temperature magnetic moment values (μ_{eff}, 298˚K) B.M, Ds, Dt, Dq^z and Dq^{xy} of Tylosin Metal complexes.

Complex	UV bands cm^{-1}/nm		Band assignment	Ds (cm^{-1})	Dt (cm^{-1})	Dq^Z (cm^{-1})	Dq^{xy} (cm^{-1})	10Dq (cm^{-1})	K_1 (cm^{-1})	μ_{eff} (B.M)	D (cm^{-1})
$[Co_2(TYS)_2Cl_2(H_2O)_4]$	ν_5	24,850 402.4	$^4A_{2g} \rightarrow {}^4E_g{}^{(c)}$	3458.6	177.14	782	1092	10920	1550	4.79	4.56
	ν_4	20,240 494	$^4A_{2g} \rightarrow {}^4B_{1g}$								
	ν_3	10,870 920	$^4A_{2g} \rightarrow {}^4E_g{}^{(b)}$								
	ν_2	9320 1073	$^4A_{2g} \rightarrow {}^4B_{2g}$								
$[Ni_2(TYS)_2Cl_2(H_2O)_4]$	ν_4	24,000 416.7	$^3B_{1g} \rightarrow {}^4E_g{}^{(d)}$	13.28	116.57	858	1062	10620	1020	3.20	2.90
	ν_3	18,480 541.1	$^3B_{1g} \rightarrow {}^3A_{2g}{}^{(c)}$								
	ν_2	10,620 941.6	$^3B_{1g} \rightarrow {}^3B_{2g}{}^{(b)}$								
	ν_1	9600 1041.7	$^3B_{1g} \rightarrow {}^3E_g{}^{(a)}$								
$[Cr_2(TYS)_2Cl_4(H_2O)_2]$	ν_4	28,110 356	$^4B_{1g} \rightarrow {}^4E_g{}^b$	3243	386	1517	2193	21930	3380	3.74	5.94
	ν_3	24,570 407	$^4B_{1g} \rightarrow {}^4A_{2g}{}^a$								
	ν_2	21,930 456	$^4B_{1g} \rightarrow {}^4B_{2g}$								
	ν_1	18,550 539	$^4B_{1g} \rightarrow {}^4E_g{}^a$								
$[Cu_2(TYS)_2Cl_2(H_2O)_4]$	ν_3	17,200 581	$^2B_{1g} \rightarrow {}^2E_g$	1510	2232	1610	2296	16100	19530	2.17	23.00
	ν_2	16,100 621	$^2B_{1g} \rightarrow {}^2B_{2g}$								
	ν_1	9770 1024	$^2B_{1g} \rightarrow {}^2A_{1g}$								
$[Fe_2(TYS)_2Cl_4(H_2O)_2]$	ν_4	27,400 364	$^6A_{1g} \rightarrow {}^4T_{1g}$ (4P)	-	-	-	-	-	-	5.60	-
	ν_3	26,100 383	$^6A_{1g} \rightarrow {}^4E_g$ (4D)								
	ν_2	24,150 414	$^6A_{1g} \rightarrow {}^4T_{2g}$ or $^4A_{1g}$ or ^4E_g (4G)								
	ν_1	17,520 571	$^6A_{1g} \rightarrow {}^4T_{1g}$ (4G)								
$[Mn_2(TYS)_2Cl_2(H_2O)_4]$	ν_4	27,610 362	$^6A_{1g} \rightarrow {}^4T_{1g}$ (4P)	-	-	-	-	-	-	5.75	-
	ν_3	26,380 379	$^6A_{1g} \rightarrow {}^4E_g$ (4D)								
	ν_2	24,410 410	$^6A_{1g} \rightarrow {}^4T_{2g}$ or $^4A_{1g}$ or ^4E_g (4G)								
	ν_1	18,060 554	$^6A_{1g} \rightarrow {}^4T_{1g}$ (4G)								

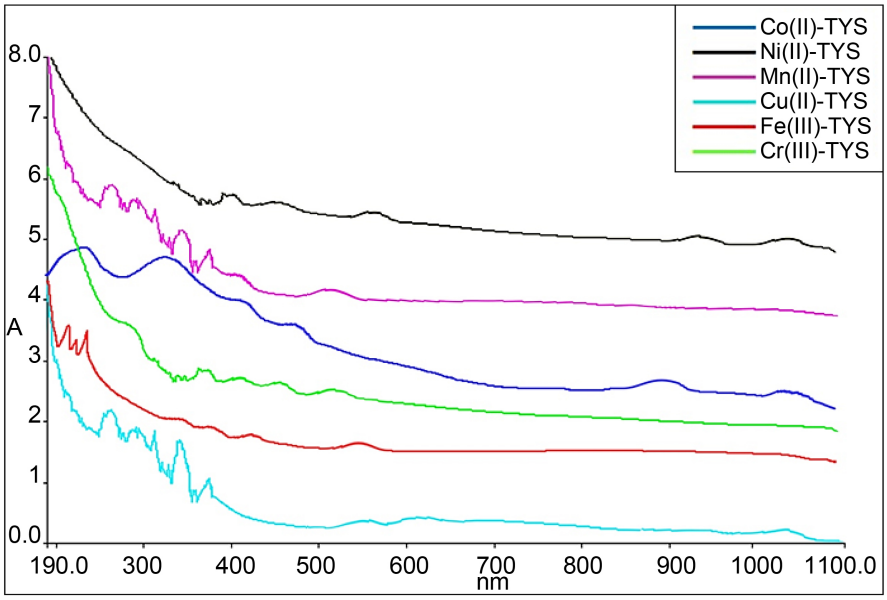

Figure 3. Showed electronic absorption spectra of different metal complexes of Tylosin.

4.3.2. Cobalt Complex

The expected calculated value of the spin only magnetic moment ($\mu_{s.o}$)of Co(II) is 3.87 B.M due to Co(II) is a d^7 system with three unpaired electrons, while the actual values of magnetic moment for complex $[Co_2(TYS)_2(Cl)_2(H_2O)_4]$ is 4.79 B.M respectively. The irregular values for Co(II)-TYS complex μ_{eff} may be attributed to $^4T_{1g}$ ground state crystal field term in octahedral symmetry which makes a significant contribution to the magnetic moment of Co(II) complex in octahedral symmetry [24]. Typically, Three absorption bands are predicted to occur in the electronic spectra of Co(II) complex with perfect high spin octahedral geometry due to three probable spin allowed transitions, $^4T_1g(F) \rightarrow {}^4T_2g(F)$, $^4T_1g(F) \rightarrow {}^4T_1g(P)$ and $^4T_1g(F) \rightarrow {}^4A_2g(F)$ that represent (ν_1), (ν_2) and (ν_3) respectively, while due to the splitting of $^4T_{1g}(F)$, ^4T_2g and $^4T_{1g}(P)$ in their electronic spectra, these cobalt complex of tylosin display four bands in their electronic spectra, as shown in (**Figure 3**), which are an evidence of axially distorted octahedral symmetry around Co(II) in these metal complexes. The electronic spectra of Co(II)-TYS complex reveal four bands, indicating axially distorted octahedral symmetry around Co(II). These bands can be ascribed to the transitions mentioned below under D_{4h} symmetry [24]:

$$\nu_1 = {}^4A_{2g} \rightarrow {}^4E_g{}^{(a)} \qquad 6/5Ds - 15/4Dt$$

$$\nu_2 = {}^4A_{2g} \rightarrow {}^4B_{2g} \qquad 8Dq + 4/5Ds - 13Dt$$

$$\nu_3 = {}^4A_{2g} \rightarrow {}^4E_g{}^{(b)} \qquad 8Dq + 4/5Ds - 17/4Dt$$

$$\nu_4 = {}^4A_{2g} \rightarrow {}^4B_{1g} \qquad 18Dq + 4/5Ds - 13Dt$$

$$\nu_5 = {}^4A_{2g} \rightarrow {}^4E_g{}^{(c)} \qquad 6Dq + 2/5Ds - 6Dt$$

$$\nu_6 = {}^4A_{2g} \rightarrow {}^4A_{2g}{}^{(a)}(P) \qquad 6Dq + 18/5Ds - 6Dt$$

The value of $Dq^{(xy)}$ has been calculated by using the derived equation $\frac{\nu_4 - \nu_2}{10}$ and D_t value has been estimated from the equation $\frac{4}{35}(\nu_3 - \nu_2)$. The common equation, $Dt = 4/7(Dq^{xy} - Dq^{z})$ used to deduce the value of Dq^{z}. The positive value of Dt and Ds produced mathematically are the indication of tetragonal elongated octahedral geometry of Co(II) complex . The smaller value of Dq^{z}, than Dq^{xy}, support and clarify the tetragonal elongation along z-axis in Co(II) complex of tylosin. The spectra for Co(II)-TYS complex shows definitely four bands at 1073, 920, 494 and 402.4 nm that correspond to the transitions (ν_2) $^4A_{2g} \rightarrow {}^4B_{2g}$, ($\nu_3$) $^4A_{2g} \rightarrow {}^4E_g^{(b)}$, ($\nu_4$) $^4A_{2g} \rightarrow {}^4B_{1g}$ and (ν_5) $^4A_{2g} \rightarrow {}^4E_g^{(c)}$,respectively. The last band ν_6 that represents the transition $^4A_{2g} \rightarrow {}^4A_{2g}^{(a)}$ (P) which may be confused with the final band appeared in the spectra. The band ν_1 refers to $^4A_{2g} \rightarrow {}^4E_g^{(a)}$ transition state that is unnoticeable due to the small gap between the two levels which causes absorption energy in the infrared range. From D_s and D_t values, the value of ν_1 has been estimated and found in 3486 cm^{-1}, which refers to the infrared spectrum.

4.3.3. Chromium Complex

The magnetic moment of Cr(III) complex of tylosin, at room temperature was found 3.74 B.M, as shown in **Table 2**, this value of Cr(III) metal complex is close to spin only value that equal 3.87 B.M thereby, suggesting an octahedral geometry around the d^3 system of chromium ion. The different values of $\mu_{s.o}$ and μ_{eff} may be an indication of distorted octahedral geometry of this complex [25]. The octahedral geometry of Cr(III)-TYS complex is determined due to the presence of three bands that represent the three lowest spin-allowed transitions $^4A_{2g} \rightarrow {}^4T_{2g}(F)$, $^4A_{2g} \rightarrow {}^4T_{1g}(F)$ and $^4A_{2g} \rightarrow {}^4T_{1g}(p)$, while four bands appeared in distorted octahedral geometry due to splitting occurred for $^4T_{2g}$ to $^4E_g{}^a$ and $^4B_{2g}$ and also scattering of $^4T_{1g}(F)$ to $^4A_{2g}{}^a$ and $^4E_g{}^b$ [26]. These four bands that represent distorted tetragonal octahedral geometry can be assigned to the following transitions.

$$\nu_1 = {}^4B_{1g} \rightarrow {}^4E_g{}^a \qquad 10Dq - 35/4Dt$$

$$\nu_2 = {}^4B_{1g} \rightarrow {}^4B_{2g} \qquad 10Dq$$

$$\nu_3 = {}^4B_{1g} \rightarrow {}^4A_{2g}{}^a \qquad 18Dq - 4Ds - 5Dt$$

$$\nu_4 = {}^4B_{1g} \rightarrow {}^4E_g{}^b \qquad 18Dq - 2Ds - 25/4Dt$$

The calculated value of Dq^{xy} is estimated from the transition ν_2 that is equal to $10Dq^{xy}$. The value of Dt is calculated by the difference between ν_1 and ν_2 which is equivalent to (35/4)Dt. The symmetry plane of Dt is related to the in-plane and out-of-plane field strengths as $Dt = 4/7(Dq^{xy} - Dq^{Z})$ which shows that Dq is in-plane (xy) and out-of-plane (z) Field strength, respectively. The parameter Ds has been calculated from the equation ($\nu_3 - \nu_2$) = 8Dq − 4Ds − 5Dt. The presence of four bands in the electronic spectral sheet of dark green chromium (III) metal

complex in the range between (350 - 550) nm is a great indication for distorted octahedral geometry. The positive value of the two field parameters Ds and Dt proved this distorted geometry. The smaller value of Dq^{xy} than Dq^{z} show axially elongated tetragonal structure for these metal complexes.

4.3.4. Copper Complex

Cu(II) complex of tylosin has shown a magnetic moment near 2.17 B.M, which corresponds to the presence of a single unpaired electron due to d^9 system of cupric ion that indicates mononuclear nature of the complex with mild paramagnetic. The difference between the spin only and magnetic moment values may be due to Strong spin orbit coupling which allows a greater value of μ_{eff} than $\mu_{S.O}$. For copper (II) metal complex of tylosin, the coordination number was six. It means that the geometry of these complexes may be distorted octahedral as tetragonal elongated structure, which can clearly determine the geometry by illustrate the electronic spectra of these Cu(II) metal complexes. In the pure octahedral coordination geometry, the ^2D state of Cu(II) is split into ^2E_g ground state and $^2T_{2g}$ excited state with a single electronic transition. Therefore, Cu(II) is no longer in the pure octahedral (Oh) geometry, and the symmetry around the metal is slightly distorted. A Jahn-Teller (J-T) distortion is taking place that changes the symmetry from octahedral (O_h) to tetragonal structure (D_{4h}) [27]. Due to the Jahn-Teller effect, the ground state ^2E_g is further scattered into $^2B_{1g}$ ground and $^2A_{1g}$ excited states, and the transition state $^2T_{2g}$ is separated into $^2B_{2g}$ ground and ^2E_g excited states. Therefore, the three bands that indicate distorted tetragonal octahedral geometry can be described by the following transitions [28]:

$$\nu_1 = {}^2B_{1g} \rightarrow {}^2A_{1g} \qquad 4Ds + 5Dt$$

$$\nu_2 = {}^2B_{1g} \rightarrow {}^2B_{2g} \qquad 10Dq$$

$$\nu_3 = {}^2B_{1g} \rightarrow {}^2E_g \qquad 10Dq + 3Ds - 5Dt$$

For Cu(II)-TYS complex, the electronic spectral exhibits clearly three bands at 9770, 16100 and 17200 cm^{-1} which can be attributed to three optical probable transitions, $^2B_{1g} \rightarrow {}^2A_{1g}$ (ν_1), $^2B_{1g} \rightarrow {}^2B_{2g}$ (ν_2) and $^2B_{1g} \rightarrow {}^2E_g$($\nu_3$). In the spectrum, there is a scattered broad band at range 580 - 625 nm that reveals scattering of $^2T_{2g}$ of octahedral geometry into $^2B_{2g}$ and ^2E_g which are close to each other [29], while the first band appeared lately at 1023 nm which assigned to $^2B_{1g} \rightarrow {}^2A_{1g}$ transition that proved distortion of axially tetragonal elongation for Cu(II) Tylosin metal complex. The value of 10Dq is estimated by determination of the second band (ν_2) at which the value of Dq^z by cm^{-1} is calculated by division of (ν_2/10). The value of Dq^{xy} is calculated directly from the popular equation that equal $Dt = 4/7(Dq^{xy} - Dq^{Z})$. The tetragonal crystal field parameters Ds and Dt founded by solving the following two equations, $\nu_3 = 4Ds + 5Dt \rightarrow (1)$ and $\nu_2 - \nu_1 = -3Ds + 5Dt \rightarrow (2)$. The same positive charge value for both parameters Ds and Dt indicated an axially elongated tetragonal geometry for both structure of Cu(II) metal complexes.

4.3.5. Iron Complex

Magnetic moments of Fe(III) metal complex was founded to be 5.60 B.M; this value is quite near to the spin-only magnetic moment corresponding to five unpaired electrons. This is due to the fact that both Fe(III) metal complexes have a high magnetic spin and are dilute octahedral complexes. Spin-orbit coupling, which limits the spin and orbital motion of electrons to an extent, could explain the somewhat lower magnetic moment value. In the electronic spectral sheet of Fe(III)-TYS complex, there were four weak bands were detected as listed in **Table 2** which attributed to the following spin forbidden transitions [30],

$$\nu_1 = {}^6A_{1g} \rightarrow {}^4T_{1g}\left(4G\right),$$

$$\nu_2 = {}^6A_{1g} \rightarrow {}^4T_{2g} \text{ or } {}^4A_{1g} \text{ or } {}^4E_g\left(4G\right),$$

$$\nu_3 = {}^6A_{1g} \rightarrow {}^4E_g\left(4D\right),$$

$$\nu_4 = {}^6A_{1g} \rightarrow {}^4T_{1g}\left(4P\right).$$

The presence of these four weak bands is indicative of axial elongated distorted octahedral geometry for these Fe(III) complexes. So, the values of different crystal field parameters have not been estimated due to the high spin nature of Fe(III) metal. The suggested geometry of the reddish brown Fe(III)-TYS complex depends on a bidentate nature of ligand, chlorides and water which allow six coordination numbers around Fe(III) that confirm distorted octahedral structure. The first bands in the UV/Vis spectra of Fe(III) which exhibits in the region range 300 - 350 nm due to ligand metal charge transfer.

4.3.6. Manganese Complex

Magnetic moments of Mn(II)-TYS complex was measured to be 5.75 B.M; the spin only magnetic moment corresponding to five unpaired electrons is very close to this value, which is attributable to the fact that Mn(II) metal complex is dilute octahedral with a high magnetic spin. The slightly low magnetic moment value could be due to spin-orbit coupling, which limits the spin and orbital motion of electrons to a small extent. The Mn(II) complex of tylosin exhibit four very weak bands that was recognized in its electronic spectral data at 18,060, 24,410, 26,380 and 27,610 cm^{-1} assigned to the following spin forbidden transitions [31], $\nu_1 = {}^6A_{1g} \rightarrow {}^4T_{1g}$ (4G), $\nu_2 = {}^6A_{1g} \rightarrow {}^4T_{2g}$ or ${}^4A_{1g}$ or ${}^4E_g$(4G), $\nu_3 = {}^6A_{1g} \rightarrow {}^4E_g$ (4D) and $\nu_4 = {}^6A_{1g} \rightarrow {}^4T_{1g}$ (4P). The presence of these weak bands is indicative of axial elongated distorted octahedral geometry for these Mn(II) complex. So, the suggested geometry of Mn(II)-TYS complex depends on a bidentate nature of ligand, chlorides and water which allow six coordination numbers around Mn(II) that confirm distorted octahedral structure.

4.3.7. Zinc Complex

For $[Zn_2(TYS)_2(H_2O)_4Cl_2]$ complex, the proposed structure due to the bidentate nature of Tylosin through oxygen atoms of OH group of mycarose sugar and Nitrogen atom of 3˚ amine group in the structure with the presence of two chloride ions and four water molecules in the inner sphere that may be a good con-

clusion for octahedral geometry of this complex. Only a high intensity band at 329 - 365 nm was observed in this complex, which was attributed to ligand metal charge transfer. No d-d transition could be observed due to the d^{10} structure of Zn(II); hence the stereochemistry could not be deduced from ultraviolet and visible spectra. However, distorted octahedral geometry is proposed for this complex based on comparisons between their spectra and those of related environments.

4.4. Electron Spin Resonance (ESR) of Cu(II)-TYS Complex

In the $[Cu_2(TYS)_2Cl_2(H_2O)_4]\cdot 25H_2O$, we have observed the relation $g_{\|} > g_{\perp} > g_e$ and the observed $g_{\|}$ and $g_{\perp}$ values which tended to be 2.43 and 2.10 ,respectively. These values are feature of Cu(II) ions coordinated by six ligands which form a distorted octahedral elongated along the z-axis. The ground state of the paramagnetic electron is $^2B_{1g}$ ($d_{x2\text{-}y2}$ state). Moreover, copper has nuclear spin 3/2 which couples with the electron spin to form four lines hyperfine splitting of the EPR spectrum (Figure 4). The nature of ligand-metal bond can ascribe according to the calculated values of α^2, β_1^2 and β^2, Table 3 indicates the covalent character of the bond. The G value is founded to be 4.5 which confirms the negligible exchange coupling takes place. The value of G can be correlated by the room temperature magnetic moment value that equals 2.17 B.M for this complex, higher than the value signs to one unpaired electron 1.73 B.M due to the orbital contribution in the spin of the complexes and confirmed that the exchange interaction is negligible. Electronic absorption spectra of $[Cu_2(TYS)_2Cl_2(H_2O)_4]\cdot 25H_2O$ showed the absorption bands $E_1(^2B_{1g} \rightarrow {}^2B_{2g})$ and

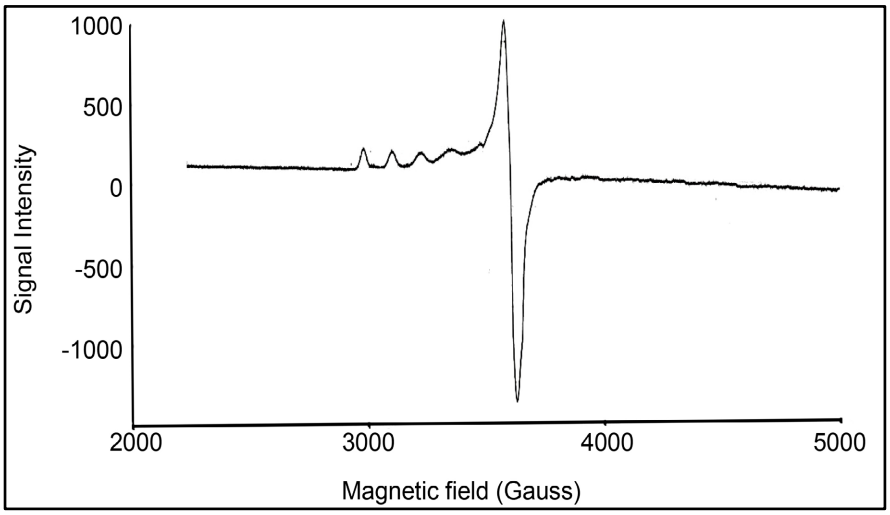

Figure 4. Showing ESR spectra of Cu(II)-TYS complex.

Table 3. Room temperature ESR spectral parameters for copper (II) complex of Tylosin.

Complex	G	$g_{\|}$	$g_{\perp}$	<g>	$A_{\|}$	$A_{\perp}$	α^2	K^2	β^2	β_1^2	$g_{\|}/A_{\|}$
$[Cu_2(TYS)_2Cl_2(H_2O)_4]\cdot 25H_2O$	4.50	2.43	2.10	2.33	65×10^4	20×10^4	0.68	0.94	0.95	098	400

$E_2(^2B_{1g} \rightarrow {}^2E_g)$ that attributed to the values 16,100 and 17,200 cm^{-1}, respectively. By comparing these values by the produced one from EPR data sheet calculations showed slightly different values as follows $E_1(^2B_{1g} \rightarrow {}^2B_{2g})$ = 15,680 cm^{-1} and $E_2(^2B_{1g} \rightarrow {}^2E_g)$ = 17,604 cm^{-1}. This correlation shows a great matching between the results of both electronic absorption spectra and EPR spectrum [32] [33] [34].

From elemental analysis, IR, electronic absorption spectra and magnetic moment values concluded structures shown in (**Figure 5** and **Figure 6**).

4.5. Thermal Analysis

The current thermal analysis study aims to learn more about the effect of temperature on metal complexes. With a heating rate of 10˚C per minute, TG/DTA analytical techniques were used to extensively study the thermal stability of the complexes. Their decline profiles are observed at different temperature ranges,

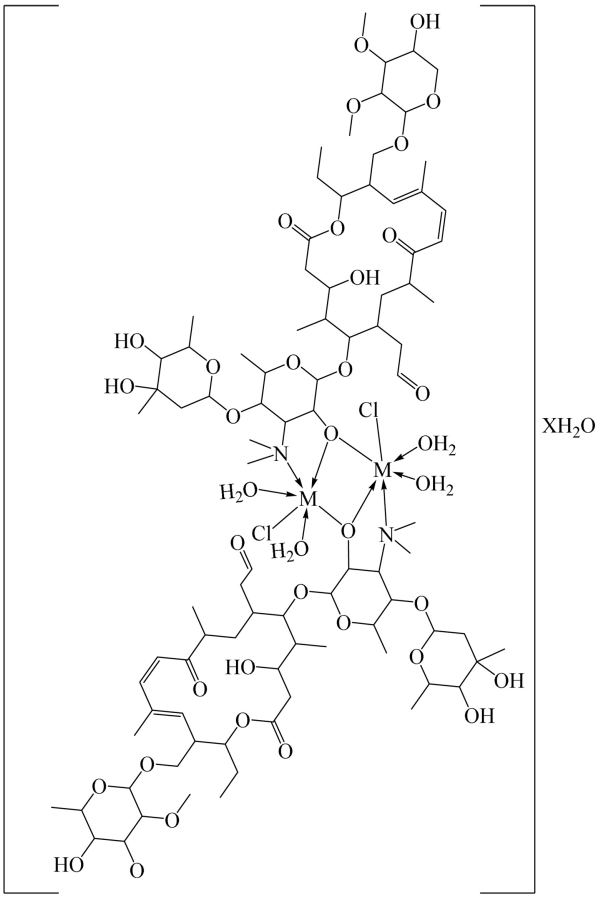

M → Metal ions, X → number of hydrated molecules of H_2O

M= Zn, X= 25H_2O → [$Zn_2(TYS)_2Cl_2(H_2O)_4$]·25H_2O	**M= Cu, X= 25H_2O → [$Cu_2(TYS)_2Cl_2(H_2O)_4$]·25H_2O**
M= Mn, X= 22.4H_2O → [$Mn_2(TYS)_2Cl_2(H_2O)_4$]·22.4H_2O	**M= Ni, X= 28.8H_2O → [$Ni_2(TYS)_2Cl_2(H_2O)_4$]·28.8H_2O**
M= Co, X= 18H_2O → [$Co_2(TYS)_2Cl_2(H_2O)_4$]·18H_2O	

Figure 5. Proposed structure of M(II)-TYS complexes, where M = Mn(II), Co(II), Ni(II), Cu(II) or Zn(II).

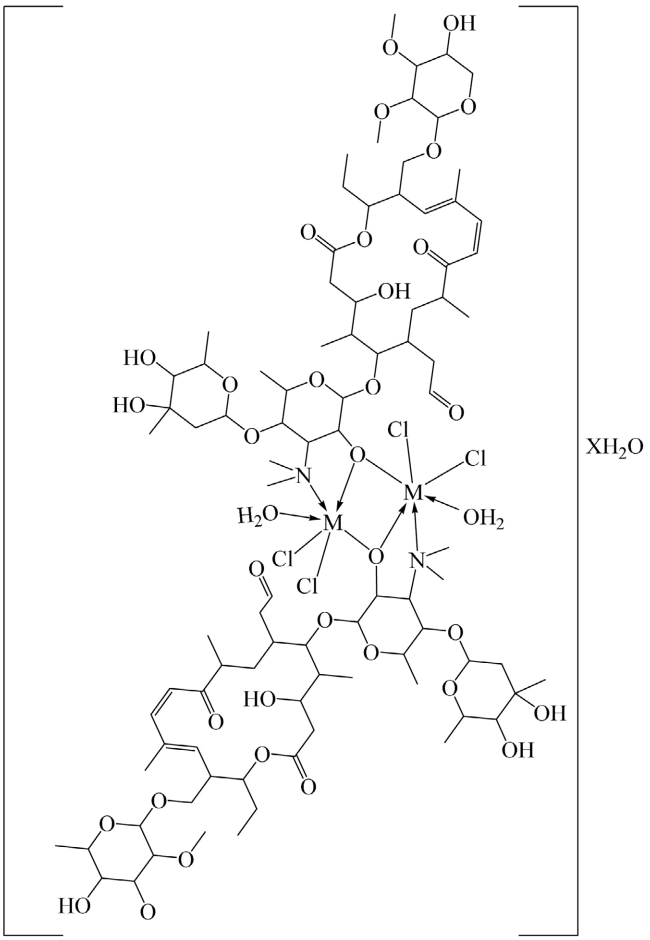

M → Metal ions, X → number of hydrated molecules of H_2O

M= Fe, X= 26H_2O → $[Fe_2(TYS)_2Cl_4(H_2O)_2]\cdot 26H_2O$, M= Cr, X= 27H_2O → $[Cr_2(TYS)_2Cl_4(H_2O)_2]\cdot 27H_2O$

Figure 6. Proposed structure of M(III)-TYS complexes, Where M = Cr(III) or Fe(III).

resulting in a variety of thermally stable products [35] [36]. The DTA/TGA signal data, **Figure 7** for the TYS ligand dedicated two peaks. The first was endothermic and the other one was exothermic with T_{max} near 83.6 and 512.4˚C and their activation energies were 20.109 and 19.226 kJ/mole, respectively. The decomposition orders are 1.58 and 0.89 which confirms that the order types are second and first, respectively. The TGA data included clearly two major steps which showed great matching with DTA data where the first step was due to the dehydration of the outer water sphere. While the other one due to the destruction of the partially dehydrated ligand with the main exit of NO_2 as a result of TYS thermal cracking. The TGA sheet indicated that TYS ligand destructed without any residue percentage, as shown in **Scheme 1**.

Both of $[Cr_2(TYS)_2Cl_4(H_2O)_2]\cdot 27H_2O$ and $[Ni_2(TYS)_2(Cl)_2(H_2O)_4]\cdot 28.8H_2O$ complexes are hydroscopic due to large number of outer water molecules as evidenced by a significant decline on TGA curve for both **Figure 8** and **Figure 9**. The DTA given data For the complex $[Cr_2(TYS)_2Cl_4(H_2O)_2]\cdot 27H_2O$ at heating

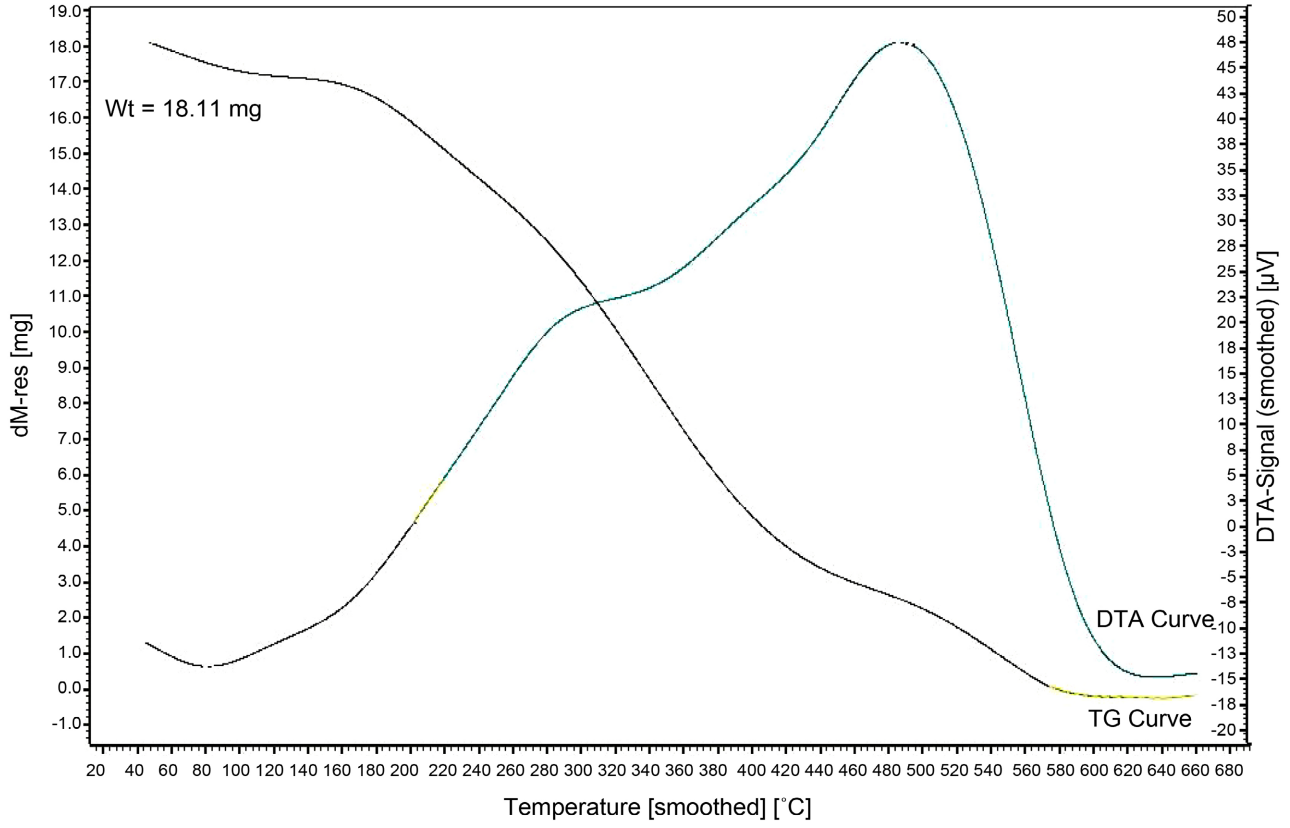

Figure 7. TG/DTA curves of TYS ligand.

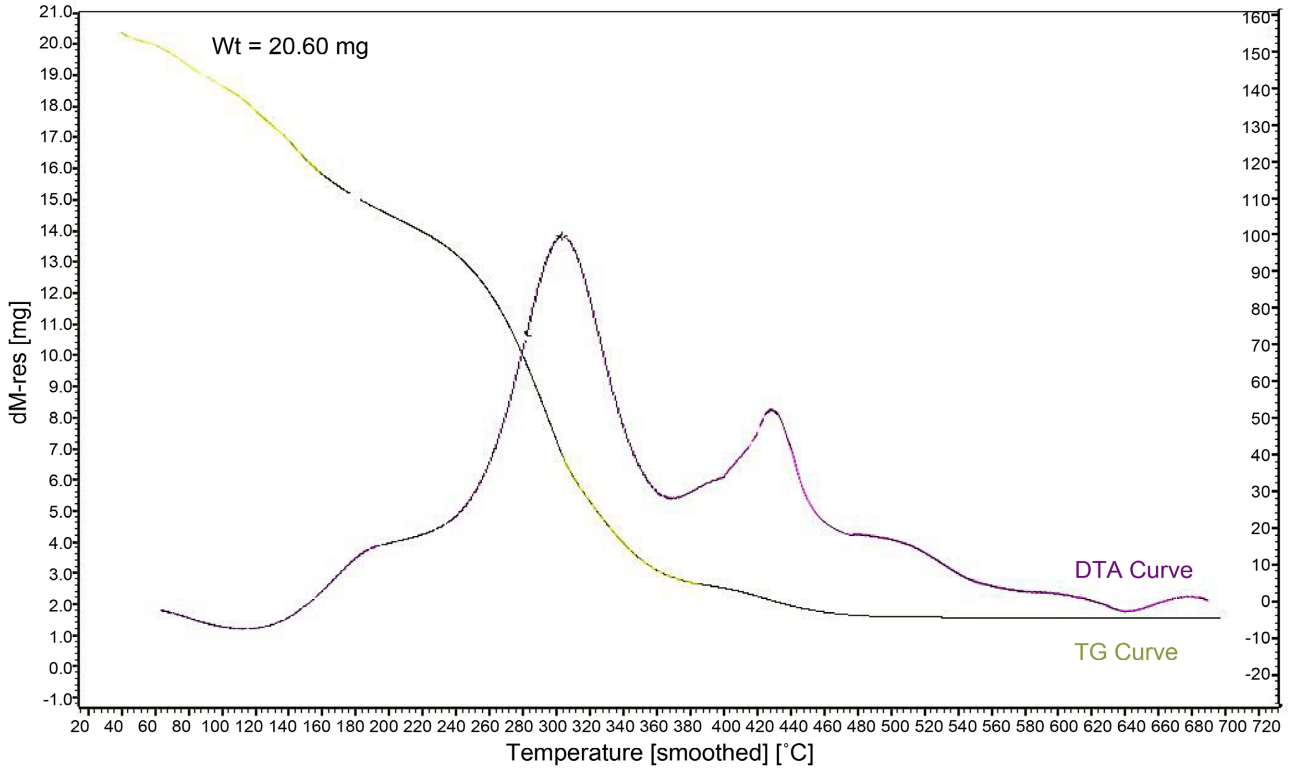

Figure 8. TG/DTA curves of $[Cr_2(TYS)_2Cl_4(H_2O)_2]\cdot 27H_2O$ complex.

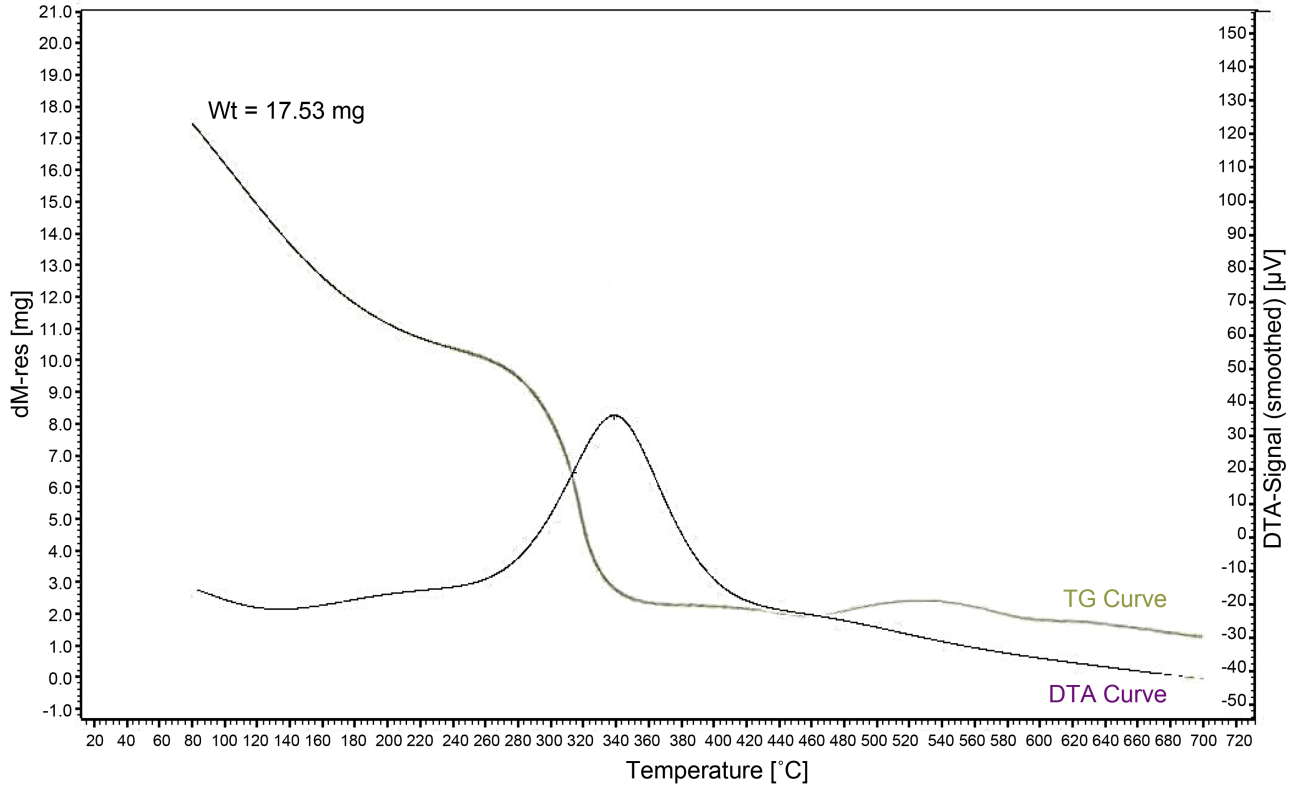

Figure 9. TG/DTA curves of $[Ni_2(TYS)_2Cl_2(H_2O)_4]\cdot 28.8H_2O$ complex.

rate 10˚C/min showed three peaks one endothermic at 116.0˚C and the others were exothermic with T_{max} 305.8˚C and 424.2˚C with activation energies 12.198, 32.903 and 92.863 KJ/mole with orders 1.38, 1.02 and 1.71, respectively. All orders are of the first type except the last one is the second type. The TG curve shows a great decline starting from temperature 46.0˚C till 184.1˚C which represents a weight loss 18.71%. This high ratio of weight loss is due to a large number of outer sphere water adsorbed molecules about 27 moles. A large number of adsorbed water in this early temperature range can be explained that this metal complex is hygroscopic type and this result is greatly confirmed with a result of Karl Fischer test. By following up the TG curve noticed the second and third steps of Cr(III) thermal cracking which agreed with TGA profile. The end of thermal cracking for $[Cr_2(TYS)_2Cl_4(H_2O)_2]\cdot 27H_2O$ complex is formation of Cr_2O_3 and remain of two carbon atom which represents by residue ratio equal 6.74%. The detailed mechanism of cracking for this complex can be shown in designated Scheme 2. Thermal analysis DTA and TGA curves, Figure 9 for $[Ni_2(TYS)_2(Cl)_2(H_2O)_4]\cdot 28.8H_2O$ complex show some variation from the given values of the other metal complex $[Cr_2(TYS)_2Cl_4(H_2O)_2]\cdot 27H_2O$ which the thermal cracking for this both complexes occurred through three steps while double decomposition steps for Ni(II)-TYS complex.

The DTA signal data for $[Ni_2(TYS)_2(Cl)_2(H2O)_4]\cdot 28.8H_2O$ complex, at a heating rate 10˚C/min gave two peaks one endothermic at T_{max} 130.0˚C and the second one exothermic at T_{max} 338.3˚C with activation energies 14.170 and 38.827

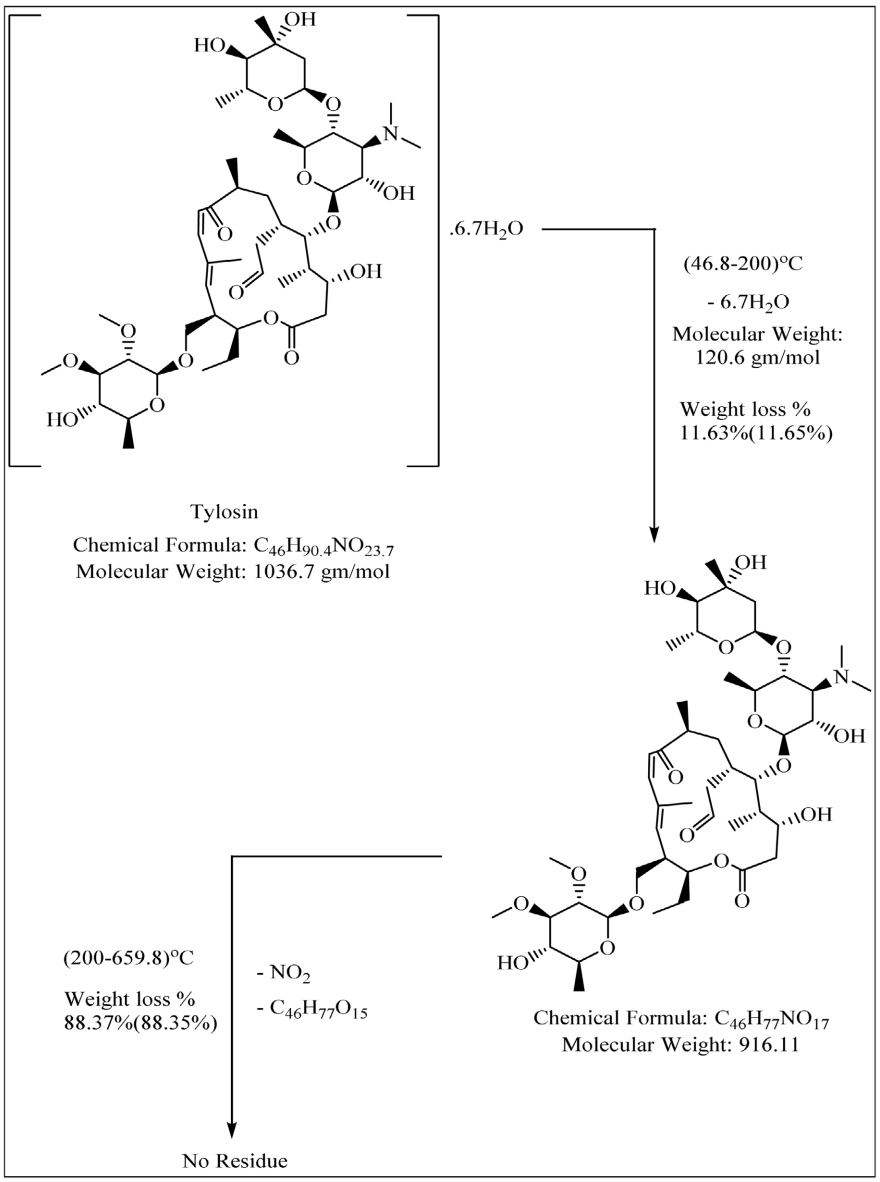

Scheme 1. Illustrated thermal cracking of Tylosin (TYS) ligand.

KJ/mole. The orders of the reactions are 1.46 and 1.40 respectively, indicating the first order for both of them. This can be demonstrated by TGA data which Ni(II) complex shows thermal stability till 79.8˚C and produced well defined two peaks at (79.8˚C - 248.0˚C), (248.0˚C - 696.6˚C) with a weight loss of 19.88% which represent the dehydration of this complex and 72.55% that describe the cracking of rest molecule except for the ratio of remained part 7.57%. The process of decomposition of the complex ended with the formation of two moles of metal oxide NiO and 4C. The decomposition technique can be shown in Scheme 3. The values of DTA thermodynamic analysis parameters of Tylosin and its metal complexes such as activation energy (ΔE^*), enthalpy of activation (ΔH^*), entropy of activation (ΔS^*) and Gibbs free energy (ΔG^*)calculated and summarized in Table 4.

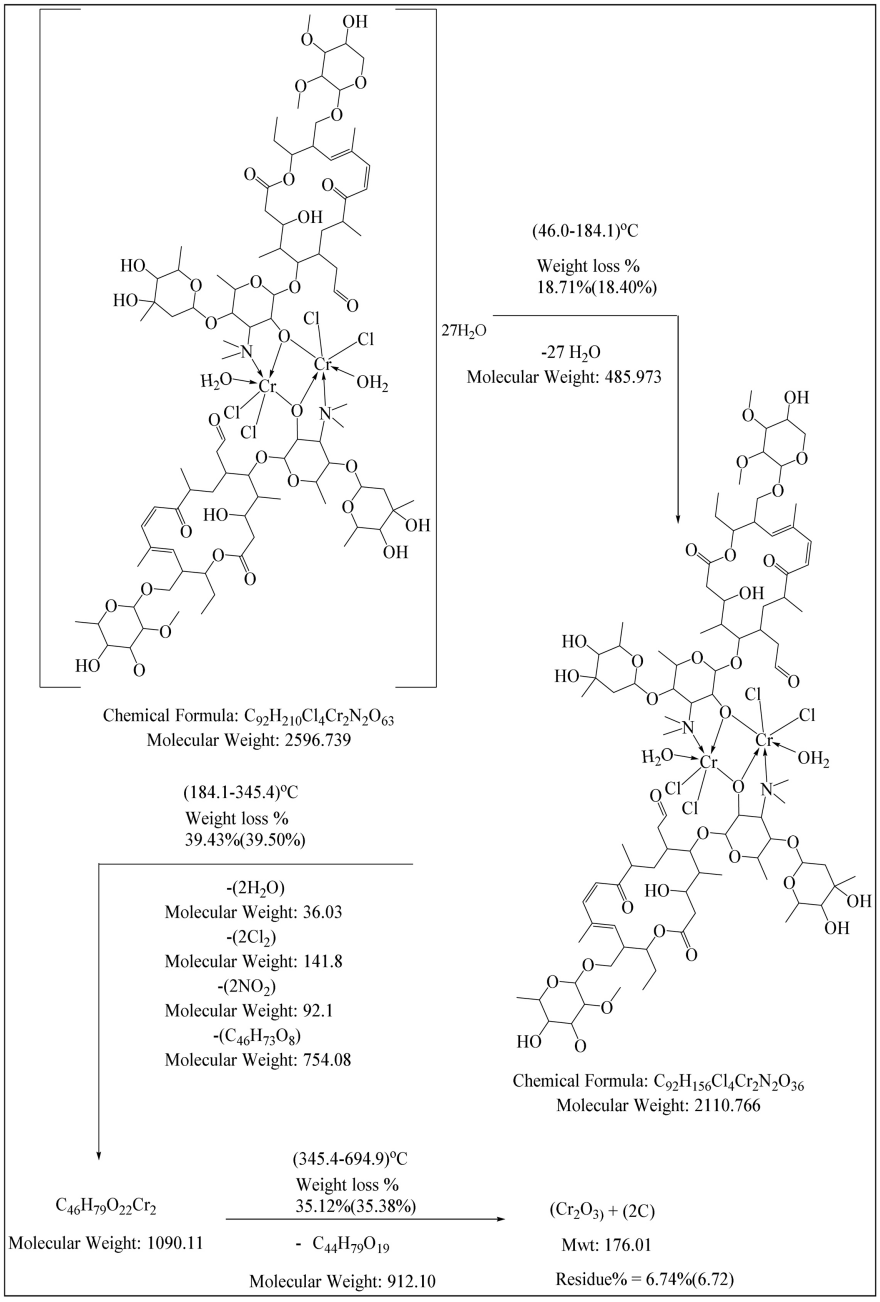

Scheme 2. Indicates steps of $[Cr_2(TYS)_2Cl_4(H_2O)_2]\cdot 27H_2O$ thermal cracking.

4.6. Biological Assessment

4.6.1. Antimicrobial Activity

Using paper disk diffusion method [37], the tylosin ligand and its synthesized metal complexes were evaluated for their antimicrobial activities. Thus, these compounds were screened against *Staphylococcus Aureus* (*S. aureus*); *Bacillus cereus* (*B. cereus*) as a Gram-positive bacteria, *Escherichia Coli* (*E. coli*); *Salmonella typhimurium* (*S. typhi*) as Gram-negative bacteria and *Candida Albicans* (*C. albicans*)as a fungal strain. The results displayed in **Table 5** clearly indicate that the free ligand has exhibited inhibition effect on all tested microorganisms

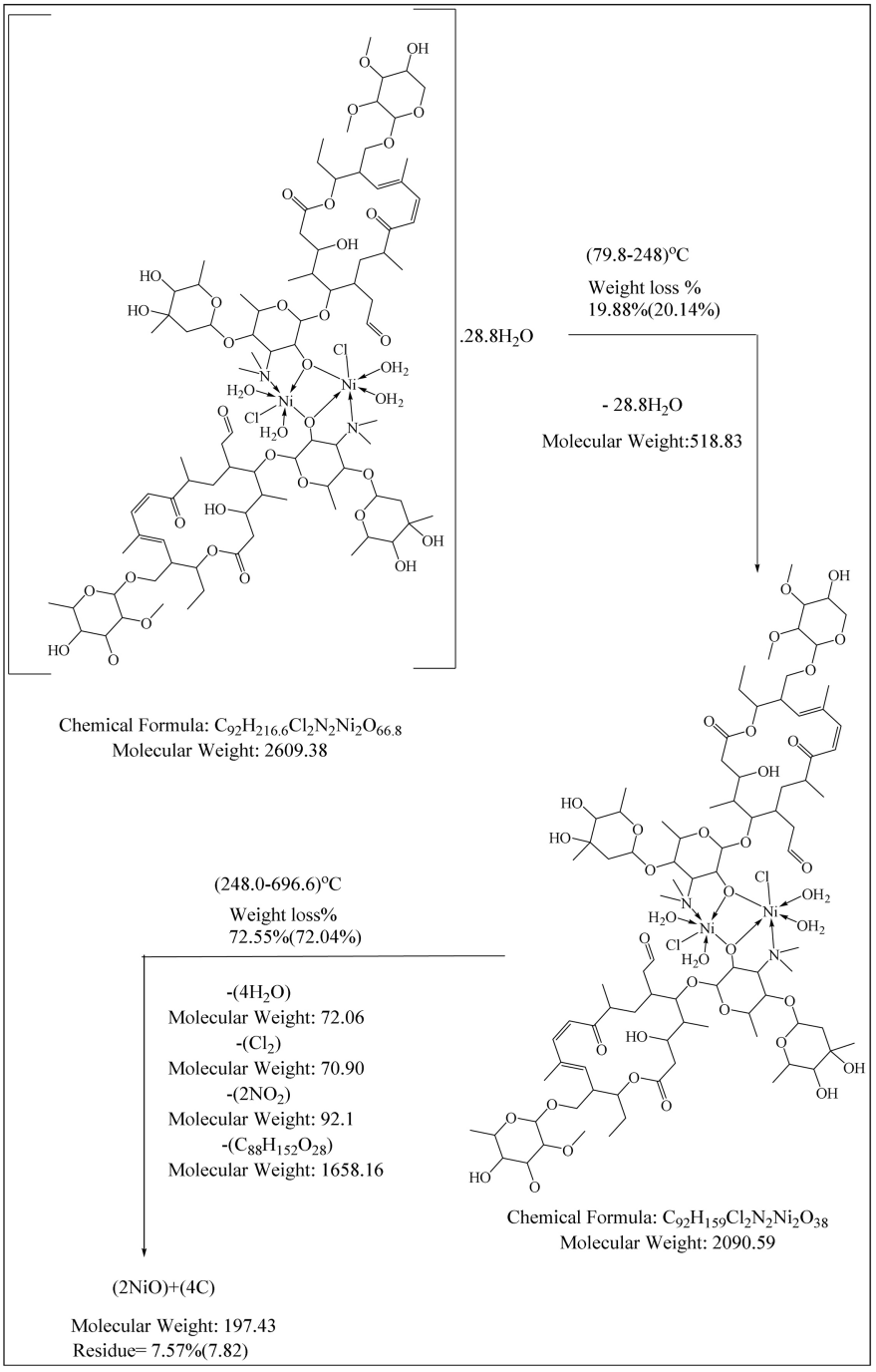

Scheme 3. Indicates steps of $[Ni_2(TYS)_2(Cl)_2(H_2O)_4]\cdot 28.8H_2O$ thermal cracking.

due to Structure-activity relationships (SAR) of tylosin that was evaluated in terms of their antimicrobial and ribosome-binding activities blocking the synthesis of protein [38].

However, the $[Zn_2(TYS)_2Cl_2(H_2O)_4]\cdot 25H_2O$ and $[Cu_2(TYS)_2Cl_2(H_2O)_4]\cdot 25H_2O$ tested compounds exhibited potent antimicrobial effect especially for Gram-positive bacterial strains (*S. aureus*); (*B. cereus*) and fungal strain (*C. albicans*) in comparison to the reference free ligand standard tylosin [38]. The

Table 4. DTA analysis parameters of Tylosin and its metal complexes.

Complex	Type	T_m (˚C)	E_a kJ mol^{-1}	N	α_m	$\Delta S^{\#}$ kJ K^{-1} mol^{-1}	$\Delta H^{\#}$ kJ mol^{-1}	Z S^{-1}	Temp. (˚C) TGA	Wt. loss%		Assignment
										Calc.	Found	
Tylosin (TYS)	Endo.	356.6	20.109	1.58	0.54	−0.28	−23.65	0.28	46.8 - 200.0	11.63	11.65	- Loss of 6.7 mole of outer sphere H_2O.
	Exo.	785.4	19.226	0.89	0.65	−0.31	−160.61	0.004	200.0 - 659.8	88.37	88.35	- Assigned to removal of NO_2 - Decomposition of the rest bulky molecule of ligand
$[Ni_2(TYS)_2Cl_2(H_2O)_4]\cdot 28.8H_2O$	Endo.	403.0	14.170	1.46	0.56	−0.29	−38.11	0.013	79.8 - 248.0	19.88	20.14	- Expected for Dehydration of almost $28.8H_2O$ molecules
	Exo.	611.3	38.827	1.40	0.56	−0.30	−101.73	0.013	248.0 - 696.6	72.55	72.04	- Elimination of coordinated $4H_2O$ and the bulky molecule of ligand with $2NO_2$ - Assigned to formation 2NiO + 2C
$[Cr_2(TYS)_2Cl_4(H_2O)_2]\cdot 27H_2O$	Endo.	389.0	12.198	1.38	0.57	−0.29	−33.93	0.012	46.0 - 184.1	18.71	18.40	- Dehydration of almost $27H_2O$ molecules
	Exo.	578.8	32.903	1.02	0.62	−0.30	−91.86	0.012	184.1 - 345.4	39.43	39.50	- Assigned to removal of $2NO_2$, two coordinated H_2O and two molecules of Cl_2. - Loss of $C_{46}H_{73}O_8$ of the bulky molecule of ligand.
	Exo.	697.2	92.863	1.71	0.52	−0.29	−126.08	0.026	345.4 - 694.9	35.12	35.38	- Elimination of the bulky molecule of ligand with formation of Cr_2O_3 + 2C

Maximum of inhibition activity (38 mm) was observed against (*S. aureus*) by Cu(II)-TYS complex. The enhanced microbial activity of zinc and copper complexes with tylosin ligand may be illustrated using chelation effect theory [39].

4.6.2. Minimum Inhibitory Concentration (MIC)

MIC is useful in research facilities because it may be used to monitor antibiotic resistance and to track the activity of new antimicrobial drugs [40]. MIC is applied for some of tylosin-Metal complexes that have highest antimicrobial activity results against tested species reported in Table 5, MIC results of ligand and its metal complexes by μg/ml are summarized in Table 6.

Table 5. Biological assessment expressed by (10 mg/ml) for free ligand tylosin and tested complexes againstbacterial strains and *Candida albicans*.

Compound	Inhibition zone diameter (mm/mg sample)				
	Gram (+) Bacterial strain		Gram (−) Bacterial strain		fungal strain
	S. aureus	*B. cereus*	*S. typhi*	*E. coli*	*C. albicans*
Tylosin (TYS.6.7H_2O) Ligand	25	20	16	17	20
$[Zn_2(TYS)_2Cl_2(H_2O)_4]\cdot 25H_2O$	36	35	16	17	28
$[Fe_2(TYS)_2Cl_4(H_2O)_2]\cdot 26H_2O$	14	16	-	14	13
$[Cr_2(TYS)_2Cl_4(H_2O)_2]\cdot 27H_2O$	16	16	10	18	13
$[Ni_2(TYS)_2Cl_2(H2O)_4]\cdot 28.8H_2O$	13	15	14	13	-
$[Co_2(TYS)_2Cl_2(H_2O)_4]\cdot 18H_2O$	13	13	16	16	-
$[Mn_2(TYS)_2Cl_2(H_2O)_4]\cdot 22.4H_2O$	12	12	19	17	-
$[Cu_2(TYS)_2Cl_2(H_2O)_4]\cdot 25H_2O$	38	21	15	18	28

Table 6. Illustrate Minimum inhibitory concentration (MIC) by (μg/ml) of tylosinbioactive metal complexes against bacterial strains and *Candida albicans*.

Compounds	Gram (+) Bacterial strain		Gram (−) Bacterial strain		Fungal strain
	S. aureus	*B. cereus*	*S. typhi*	*E. coli*	*C. albicans*
Tylosin (TYS.6.7H_2O) Ligand	31.25	62.5	250	250	62.5
$[Zn_2(TYS)_2Cl_2(H_2O)_4]\cdot 25H_2O$	31.25	15.625	15.625	15.625	125
$[Fe_2(TYS)_2Cl_4(H_2O)_2]\cdot 26H_2O$	250	125	250	250	250
$[Cr_2(TYS)_2Cl_4(H_2O)_2]\cdot 27H_2O$	500	15.625	1000	500	500
$[Cu_2(TYS)_2Cl_2(H_2O)_4]\cdot 25H_2O$	31.25	15.625	15.625	15.625	125

$[Zn_2(TYS)_2Cl_2(H_2O)_4]\cdot 25H_2O$ and $[Cu_2(TYS)_2Cl_2(H_2O)_4]\cdot 25H_2O$ complexes revealed low concentration value of MIC results with *S. aureus* with the same value for both 31.25 μg/ml. For *B. cereus* species both novels tested complexes Zn(II)-TYS and Cu(II)-TYS show lower MIC values with higher antimicrobial activity with value 15.625 μg/ml. Both tested metal complexes of tylosin possess the highest activity with the lowest or equal concentration rather than the tylosin ligand that is sufficient to make the effect of bacterial inhibition.

Free macrolide ligandtylosin show lower MIC value for the fungal strain *Candida albicans* with value 62.5 μg/ml than two complexes, Zn(II)-TYS and Cu(II)-TYS which poses the highest antifungal activity has the same MIC value by 125 μg/ml. It means that the ligand has better MIC value than Zn(II)-TYS and Cu(II)-TYS complexes although both complexes have higher antifungal activity than tylosin ligand.

5. Conclusion

Elemental analysis and spectroscopic measurements of IR, UV/Vis, and ESR are applied to prove the structures of novel tylosin metal chelates, which are then

confirmed by thermal analyses. The analytical results were used to determine the stoichiometry of complexes. Spectroscopic Elucidation of complexes confirms tetragonal distortion geometries. An ESR spectrum of copper was studied for Cu(II)-TYS complex, which is compatible with electronic studies. The spectral data confirmed that tylosin acts as a bidentate ligand. The kinetic and thermodynamic parameters were calculated from the differential thermal analysis curves. Some complexes showed highly antibacterial and antifungal activity against some strains than free ligand. The value of MIC concluded that these metal complexes [Zn(II) and Cu(II)] could be used as effective drugs in killing bacteria and fungi in the field of pharmaceutical applications.

Conflicts of Interest

The authors declare no conflicts of interest regarding the publication of this paper.

References

[1] Khaliq, S., Akhtar, K., AfzalGhauri, M., *et al*. (2009) Change in Colony Morphology and Kinetics of Tylosin Production after UV and Gamma Irradiation Mutagenesis of *Streptomyces fradiae* NRRL-2702. *Microbiological Research*, **164**, 469-477. https://doi.org/10.1016/j.micres.2007.02.005

[2] Baltz, R.H. and Seno, E.T. (1988) Genetics of *Streptomyces fradiae* and Tylosin Biosynthesis. *Annual Review of Microbiology*, **42**, 547-574. https://doi.org/10.1146/annurev.mi.42.100188.002555

[3] Loftin, K.A., Adams, C.D., Meyer, M.T. and Surampalli, R. (2008) Effects of Ionic Strength, Temperature, and pH on Degradation of Selected Antibiotics. *Journal of Environmental Quality*, **37**, 378-386. https://doi.org/10.2134/jeq2007.0230

[4] Fish, S.A. and Cundliffe, E. (1996) Structure-Activity Studies of Tylosin-Related Macrolides. *The Journal of Antibiotics*, **49**, 1044-1048. https://doi.org/10.7164/antibiotics.49.1044

[5] Huang, G., Okabe, M., Kahar, P., Tsunekawa, H. and Park, Y. (2001) Optimization of Tylosin Feeding Rate Profile in Production of Acetyl-Isovaleryl Tylosin (AIV) from Tylosin by *Streptomyces thermotolerans* YN554. *Journal of Bioscience and Bioengineering*, **91**, 504-508. https://doi.org/10.1016/S1389-1723(01)80281-4

[6] Vladimirova, E.V., Dunaeva, A.A., Shipulo, E.V., *et al*. (2011) Studies of Complex Formation between Macrolide Antibiotics and Alkali and Alkali—Earth Metals by the Voltammetry at the Interface of Two Immiscible Electrolyte Solutions. *Russian Journal of Electrochemistry*, **47**, 361-368. https://doi.org/10.1134/S1023193510121031

[7] Lan, C., Yin, D., Yang, Z., Zhao, W., Chen, Y., Zhang, W. and Zhang, S. (2019) Determination of Six Macrolide Antibiotics in Chicken Sample by Liquid Chromatography-Tandem Mass Spectrometry Based on Solid Phase Extraction. *Journal of Analytical Methods in Chemistry*, **2019**, Article ID: 6849457. https://doi.org/10.1155/2019/6849457

[8] Prats, C., Francesch, R., Arboix, M. and Perez, B. (2002) Determination of Tylosin Residues in Different Animal Tissues by High Performance Liquid Chromatography. *Journal of Chromatography B, Analytical Technologies in the Biomedical and Life Sciences*, **766**, 57-65. https://doi.org/10.1016/S0021-9673(01)01325-5

[9] Yaneva, Z., Georgieva, N., Koinarski, V. and Petrova, D. (2015) Rapid RP HPLC Method with PDA Detection for Tylosin Determination in Liquid Samples. *Trakia Journal of Sciences*, **13**, 309-314. https://doi.org/10.15547/tjs.2015.s.02.066

[10] Przeniosło-Siwczyńska, M., Grelik, A. and Kwiatek, K. (2020) Identification and Quantification of Tylosin in Animal Feed by Liquid Chromatography Combined with Electrospray Ionisation Mass Spectrometry. *Veterinary Research*, **64**, 299-304. https://doi.org/10.2478/jvetres-2020-0031

[11] Keskar, M.R. and Jugade, R.M. (2015) Spectrophotometric Investigations of Macrolide Antibiotics: A Brief Review. *Analytical Chemistry Insights*, **10**, 29-37. https://doi.org/10.4137/ACI.S31857

[12] Sarmah, A.K., Meyer, M.T. and Boxall, A.B. (2006) A Global Perspective on the Use, Sales, Exposure Pathways, Occurrence, Fate and Effects of Veterinary Antibiotics (VAs) in the Environment. *Chemosphere*, **65**, 725-759. https://doi.org/10.1016/j.chemosphere.2006.03.026

[13] Caldwell, J.R. and Moyer, H.V. (1935) Determination of Chloride: A Modification of the Volhard Method. *Industrial & Engineering Chemistry Analytical*, **7**, 38-39. https://doi.org/10.1021/ac50093a018

[14] Bradley, K.B. and Potts, W.J. (1958) The Internally Standardized Nujol Mull as a Method of Quantitative Infrared Spectroscopy. *Applied Spectroscopy*, **12**, 77-80. https://doi.org/10.1366/000370258774615465

[15] Fouad, D., Bayoumi, A., ElGahami, M., Ibrahim, S. and Hammam, A. (2010) Synthesis and Thermal Studies of Mixed Ligand Complexes of Cu(II), Co(II), Ni(II) and Cd(II) with Mercaptotriazoles and Dehydroacetic Acid. *Natural Science*, **2**, 817-827. https://doi.org/10.4236/ns.2010.28103

[16] Clinical and Laboratory Standards Institute (CLSI) (2017) Performance Standards for Antimicrobial Susceptibility Testing. M100, 27th Edition, Replaces M100-S26.

[17] Khalifa, R.A., Nasser, M.S., Gomaa, A.A., Osman, N.M. and Salem, H.M. (2013) Resazurin Microtiter Assay Plate Method for Detection of Susceptibility of Multidrug Resistant *Mycobacterium tuberculosis* to Second-Line Anti-Tuberculous Drugs. *Egyptian Journal of Chest Diseases and Tuberculosis*, **62**, 241-247. https://doi.org/10.1016/j.ejcdt.2013.05.008

[18] Sarker, S.D., Nahar, L. and Kumarasamy, Y. (2007) Microtitre Plate-Based Antibacterial Assay Incorporating Resazurin as an Indicator of Cell Growth, and Its Application in the *in Vitro* Antibacterial Screening of Phytochemicals. *Methods*, **42**, 321-324. https://doi.org/10.1016/j.ymeth.2007.01.006

[19] De Freitas, A.G.M., Minho, L.A.C., de Magalhaes, B.E.A., Dos Santos, W.N.L., Santos, L.S. and Fernandes, S.A.D. (2021) Infrared Spectroscopy Combined with Random Forest to Determine Tylosin Residues in Powdered Milk. *Food Chemistry*, **365**, Article ID: 130477. https://doi.org/10.1016/j.foodchem.2021.130477

[20] De Freitas, A.G., de Magalhães, B.E., Minho, L.A., Leão, D.J., Santos, L.S. and Augusto de Albuquerque Fernandes, S. (2021) FTIR Spectroscopy with Chemometrics for Determination of Tylosin Residues in Milk. *Journal of the Science of Food and Agriculture*, **101**, 1854-1860. https://doi.org/10.1002/jsfa.10799

[21] Yin, Y.Y., Guo, X.T. and Peng, D. (2018) Iron and Manganese Oxides Modified Maize Straw to Remove Tylosin from Aqueous Solutions. *Chemosphere*, **205**, 156-165. https://doi.org/10.1016/j.chemosphere.2018.04.108

[22] Martin, L.Y., Sperati, C.R. and Busch, D.H. (1977) The Spectrochemical Properties of Tetragonal Complexes of High Spin Nickel(II) Containing Macrocyclic Ligands. *Journal of the American Chemical Society*, **99**, 2968-2981.

https://doi.org/10.1021/ja00451a020

[23] Ranjan, R., Rani, R., Suman Singh, S., Singh, A.K. and Sharma, S. (2010) Tetragonal Distortion Parameter of Some Nickel(II) Complexes. *Asian Journal of Chemistry*, **22**, 7580-7584.

[24] Kumar, D., Singh, A.K., Kumar, A., Prasad, D., Kumar, V. and Sharma, S. (2020) Synthesis, Spectral Characterization and Biological Activity of Metal(II) Complexes of 2,4,5-Trimethoxybenzaldehyde-S-Benzyldithiocarbazone. *Asian Journal of Chemistry*, **32**, 209-214. https://doi.org/10.14233/ajchem.2020.22476

[25] Chandra, S. and Pipil, P. (2014) Synthesis, Spectral Characterization and Biological Evaluation of Chromium(III) Complexes of Schiff Base. *Open Journal of Inorganic Chemistry*, **4**, 30-40. https://doi.org/10.4236/ojic.2014.42005

[26] Choi, J.-H., Oh, I.-G., Lee, S.H. and Park, Y.C. (2003) Electronic Spectroscopy and Ligand Field Analysis of trans-$[CrX_2([15]aneN_4)]^+$ (X = F, CI). *Journal of the Korean Chemical Society*, **47**, 109-114. https://doi.org/10.5012/jkcs.2003.47.2.109

[27] Chakradhar, R.P., Sreekanth, Ramesh, K.P., Rao, J.L. and Ramakrishna, J. (2003) Mixed Alkali Effect in Borate Glasses—Electron Paramagnetic Resonance and Optical Absorption Studies in Cu^{2+} Doped xNa_2O-(30-x)K_2O-70B_2O_3 Glasses. *Journal of Physics*: *Condensed Matter*, **15**, 1469-1486.

[28] Halcrow, M.A. (2013) Jahn-Teller Distortions in Transition Metal Compounds, and Their Importance in Functional Molecular and Inorganic Materials. *Chemical Society Reviews*, **42**, 1784-1795. https://doi.org/10.1039/C2CS35253B

[29] Reinen, D., Atanasov, M., Köhler, P. and Babel, D. (2010) Jahn-Teller Coupling and the Influence of Strain in T_g and E_g Ground and Excited States—A Ligand Field and DFT Study on Halide $M^{III}X_6$ Model Complexes [M = Ti^{III}-Cu^{III}; X = F^-, Cl^-]. *Coordination Chemistry Reviews*, **254**, 2703-2754. https://doi.org/10.1016/j.ccr.2010.04.015

[30] Birendra, K., Kumar, B., Kumar, S., Kumar, D. and Sharma, S. (2017) Synthesis and Characterization of Manganese, Copper and Zinc Complexes Derived from Schiff-Base Ligand. *Oriental Journal of Chemistry*, **33**, 2643-2646. https://doi.org/10.13005/ojc/330563

[31] Navneetsinha, R., Singh, V.P., Kumar, D. and Sharma, S. (2021) Spectroscopic Elucidation of Some Complexes of Vanillin Semicarbazone. *Oriental Journal of Chemistry*, **37**, 826-832. https://doi.org/10.13005/ojc/370409

[32] El-Boraey, H.A. and Serag El-Din, A.A. (2014) Transition Metal Complexes of a New 15-membered[N5]penta-azamacrocyclic Ligand with Their Spectral and Anticancer Studies. *Spectrochimica Acta Part A*: *Molecular and Biomolecular Spectroscopy*, **132**, 663-671. https://doi.org/10.1016/j.saa.2014.05.018

[33] Rosu, T., Negoiu, M., Pasculescu, S., Pahontu, E., Poirier, D. and Gulea, A. (2010) Metal-Based Biologically Active Agents: Synthesis, Characterization, Antibacterial and Antileukemia Activity Evaluation of Cu(II), V(IV) and Ni(II) Complexes with Antipyrine-Derived Compounds. *European Journal of Medicinal Chemistry*, **45**, 774-781. https://doi.org/10.1016/j.ejmech.2009.10.034

[34] Kozlevčar, B. and Šegedin, P. (2008) Structural Analysis of a Series of Copper(II) Coordination Compounds and Correlation with Their Magnetic Properties. *Croatica Chemica Acta*, **81**, 369-379.

[35] Hassan, F.S.M., Kuran, W.S., Ibrahim, A.A. and Adam, F.A. (2020) Synthesis, Characterization and Biological Activity of Sodium Barbitone-GroupVIII Metals (viz. Ni(II), Pd(II) and Pt(II)) Complexes. *Open Journal of Inorganic Nonmetallic Materials*, **10**, 1-14. https://doi.org/10.4236/ojinm.2020.101001

[36] Arouri, A., Dridi, R., Kefi, R. and Zid, M.F. (2021) Structural Study, Vibrational, Optical, Thermal Properties and Hirshfeld Surface Analysis of a New Iron(III) Complex: $FeCl_4(C_5N_2H_6)(C_5N_2H_5)$. *Crystal Structure Theory and Applications*, **10**, 14-26. https://doi.org/10.4236/csta.2021.101002

[37] El-Sherbiny, G.M., Moghannem, S.A. and Sharaf, M.H. (2017) Antimicrobial Activities and Cytotoxicity of Sisymbriumirio L Extract against Multi-Drug Resistant Bacteria (MDRB) and *Candida albicans*. *International Journal of Current Microbiology and Applied Sciences*, **6**, 1-13. https://doi.org/10.20546/ijcmas.2017.604.001

[38] Naranda, A., Suskovic, B., Kelneric, Z. and Djokic, S. (1994) Structureactivity Relationship among Polyhydro Derivatives of Tylosin. *The Journal of Antibiotics*, **47**, 581-587. https://doi.org/10.7164/antibiotics.47.581

[39] Karim, A., Rani, R., Ranjan, R., Kumar, U., Kumar, V. and Sharma, S. (2017) Synthesis, Characterization and Biocidal Properties of Oxovanadium Complexes. *Asian Journal of Chemistry*, **29**, 626-630. https://doi.org/10.14233/ajchem.2017.20286

[40] Bollela, V., Sato, D. and Fonseca, B. (1999) McFarland Nephelometer as a Simple Method to Estimate the Sensitivity of the Polymerase Chain Reaction Using *Mycobacterium tuberculosis* as a Research Tool. *Brazilian Journal of Medical and Biological Research*, **32**, 1073-1076. https://doi.org/10.1590/S0100-879X1999000900003